Appl. Phys. A 73, 741–747 (2001) / Digital Object Identifier (DOI) 10.1007/s003390100887

Applied Physics A
Materials
Science & Processing

Short-laser-pulse-driven emission of energetic ions into a solid target from a surface layer spalled by a laser prepulse

A.G. Zhidkov[1,4], **L.V. Zhigilei**[2,*], **A. Sasaki**[1], **T. Tajima**[3]

[1] Advanced Photon Research Center, JAERI, 25-1 Mii-minami-machi, Neyagawa, Osaka, 572-0019, Japan
[2] Department of Materials Science and Engineering, University of Virginia, Charlottesville, Virginia 22903, USA
[3] Lawrence Livermore National Laboratory, L-441, Livermore, CA 94551, USA
[4] General Physics Institute, 117945, Vavilov, 38, Moscow, Russia

Received: 13 March 2001/Accepted: 20 March 2001/Published online: 20 June 2001 –

Abstract. An efficient emission of picosecond bunches of energetic protons and carbon ions from a thin layer spalled from a organic solid by a laser prepulse is demonstrated numerically. We combine the molecular dynamics technique and multi-component collisional particle-in-cell method with plasma ionization to simulate the laser spallation and ejection of a thin ($\sim$ 20–30 nm) solid layer from an organic target and its further interaction with an intense femtosecond laser pulse. In spite of its small thickness, a layer produced by laser spallation efficiently absorbs ultrashort laser pulses with the generation of hot electrons that convert their energy to ion energy. The efficiency of the conversion of the laser energy to ions can be as high as 20%, and 10% to MeV ions. A transient electrostatic field created between the layer and surface of the target is up to 10 GV/cm.

PACS: 79.20.Ds; 61.80.Az; 52.40; 02.70.Ns

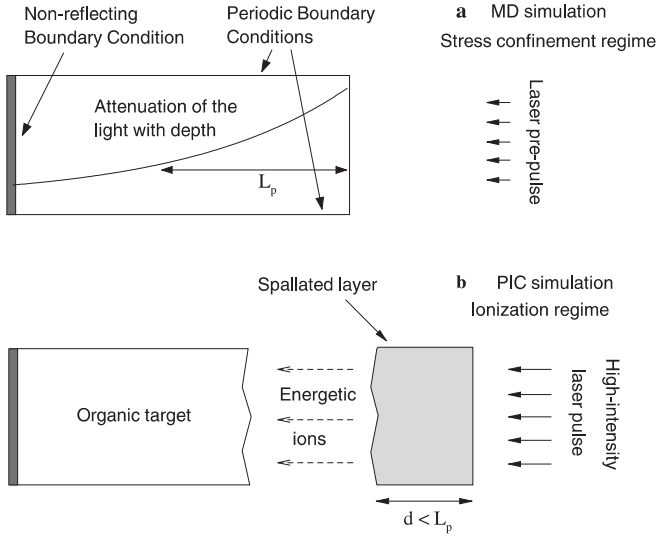

Fig. 1a,b. Schematic sketch of the simulation setup

Thin foil targets irradiated by short intense laser pulses can be efficient sources of energetic ions with a low emittance [1, 2]. Such sources may be adopted for ion accelerators or used directly in various applications ranging from materials physics and chemistry to nuclear physics. In particular, experimental studies of the excitation of low-lying (1–20 keV) isomeric nuclei levels [3, 4] and stimulation of resonance reactions with a few MeV threshold in a short-lived nucleus [5] can be realized with the laser plasma ion source. The high-current picosecond beam of MeV ions produced by a short laser pulse near a target surface may be a good tool for the investigation of physical and chemical processes in a transient medium, such as short-living isotopes or rapidly modified solids.

Although energetic ions appear from a thin foil in both directions, the use of the forward, as shown in Fig. 1, ion acceleration is more practical allowing us to sustain a high current on a target. Two mechanisms of the forward ion acceleration by a short laser pulse have been discussed [1, 2, 6–14]. The first mechanism is the ion acceleration from the front side of an irradiated foil that is dominated by the charge separation due to the ponderomotive force [6, 13]. The second one is the hot-electron-driven ion acceleration [1, 2, 11, 14] from the rear side of the foil. While the first mechanism is inefficient in overdense plasmas because the potential difference produced by the ponderomotive force rapidly decreases with the plasma density [11], the second one needs a plasma boundary at the rear side of a target with a thickness comparable to the excursion length of hot electrons. Moreover, the ion source must be near the target surface to shorten the duration of the high-current ion beam. In particular, if the distance between the source and the target is 1 μm, the duration of the beam of ions with energy over 100 keV can be shorter than 1 ps.

The ability to produce a layer of material or large clusters in the vicinity of a target is, therefore, a critical step in creation of an efficient source of energetic ions directed toward the target surface. One can expect that much more energetic ions can be produced from such a layer as compared to an intact target with plasma corona [13]. The crucial point is the layer thickness. The layer should be not trans-

*Corresponding author.

parent and not thick to let hot electrons to pass through. In this work, we suggest the use of laser spallation of the target by a low intensity laser prepulse as a method for the generation of a well-defined layer of solid or liquid material above the target surface. The ejection of liquid and/or solid particulates of different sizes has been observed in laser ablation both experimentally [15–19] and in molecular dynamics simulations [20, 21] for a variety of target materials. It has been also discussed in a number of works [21–23] that the ejection of a large and relatively intact layer of material can be achieved under conditions of stress confinement [21–24], when photomechanical effects driven by the relaxation of the laser induced stresses contribute to the material ejection. In particular, observations from scattering experiments for laser ablation of polymer targets by Hare et al. [22] suggest that photomechanical effects can lead to the ejection of a relatively intact layer of material that maintains its integrity at least on the timescale of tens of nanoseconds. Such a layer moving several micrometers apart from the target and being irradiated further by a femtosecond laser pulse could serve as an efficient contact source of energetic ions.

The experimental setup proposed and explored computationally in this work involves two distinct stages with fundamentally different physics governing the laser-induced processes. First, a prepulse with intensity that is above the threshold for the collective material ejection (ablation) but significantly lower than the intensities needed for ionization is used to cause the ejection of large clusters or spallation of a thin layer of target material. At this stage the processes induced by laser irradiation have thermal and/or photomechanical character and ionization can be neglected (fraction of ions in the plume has been estimated to be $\sim 10^{-4}$ in this irradiation regime [25]). Second, the layer or the large clusters are irradiated with an intense femtosecond laser pulse producing hot electrons that dominate the emission of energetic ions. Clearly, the processes of thermal ablation or photomechanical spallation and short-pulse-laser–plasma interaction cannot be described within a single computational approach. A hybrid computational technique that combines the classical molecular dynamics (MD) method for simulation of the ablation/spallation by the laser prepulse and the multi-component collisional particle-in-cell (PIC) method with plasma ionization to model the ion emission from the layer irradiated by the second pulse is illustrated by Fig. 1. Below we discuss the spallation regime only, although the cluster ejection in the regime of thermal ablation [20, 23] may give an advance in the laser absorption rate and hot electron production as well [26].

1 Computational method

1.1 MD model for laser ablation

The simulation of laser ablation of an organic target is performed using the breathing sphere model that has been described in detail in [27]. Briefly, the model assumes that each molecule (or an appropriate group of atoms) can be represented by a single particle that has the true translational degrees of freedom but an approximate internal degree of freedom. This internal (breathing) mode allows one to reproduce a realistic rate of the conversion of internal energy of the molecules excited by the laser to the translational motion of the other molecules. Since the molecules rather than the atoms are the particles of interest in the model, the system size can be large enough to model the collective dynamics leading to laser ablation and damage. Moreover, since we are not following high-frequency atomic vibrations, we can use a much longer timestep in the numerical integration and keep track of the processes in the simulated system for a longer time.

The system chosen for modeling of laser ablation is a molecular solid. The parameters of the intermolecular potential are chosen to represent the van der Waals interaction in a molecular solid with the cohesive energy of 0.6 eV, elastic bulk modulus of ~ 5 GPa, and density of $1.2\,\mathrm{g/cm^3}$. A mass of 100 Daltons is attributed to each molecule. A computational cell of dimensions $40 \times 10 \times 90$ nm (253 808 molecules) is used and periodic boundary conditions in the directions parallel to the surface are imposed, Fig. 1a. These conditions simulate the situation in which the laser spot diameter is large compared to the penetration depth so that the effects of the edges of the laser beam are neglected. At the bottom of the MD computational cell we apply the dynamic boundary condition developed to avoid artifacts due to reflection of the laser-induced pressure wave from the boundary of the computational cell, Fig. 1a. The boundary condition accounts for the laser-induced pressure-wave propagation as well as the direct laser energy deposition in the boundary region and is described in [28].

The laser irradiation is simulated by vibrational excitation of molecules that are randomly chosen during the laser pulse duration. The probability of a molecule to be excited is modulated by Lambert–Beer's law to reproduce the exponential attenuation of the laser light with depth, Fig. 1a, with an absorption depth of 50 nm. The vibrational excitation is modeled by depositing a quantum of energy equal to the photon energy into the kinetic energy of internal motion of a given molecule. Irradiation at a wavelength of 337 nm (3.68 eV) is simulated in this study. The total number of photons entering the model during the laser pulse is determined by the laser fluence. The value of the laser pulse duration, 15 ps, is chosen in order to make sure that the simulations are performed in the regime of stress confinement for which spallation and ejection of a layer of material can be expected [21–23].

1.2 Particle-in-cell method with plasma ionization

We apply a collisional particle-in-cell (PIC) method with plasma ionization to simulate the interaction of a thin layer produced as a result of the laser-induced spallation with an intense femtosecond laser pulse. The method is based on the collisional electromagnetic PIC and is appropriate for the analysis of the dynamics of a solid density plasma created by a femtosecond *p*-polarized, obliquely incident laser pulse. The method employs the Langevin equation to account for elastic collisions and non-local-thermodynamic-equilibrium average ion model for plasma ionization including the ionization due to the laser as well as plasma field. The method conforms to a direct solution of the Fokker–Planck equation [29]. The details of the method can be found in [30]. To

solve the Maxwell equations for a p-polarized obliquely incident laser pulse, we use the two-waves approximation [30]. We include ionization processes in the PIC simulation by allowing the change of computational particle (CP) charges. A change in the charge of CPs representing plasma electrons is calculated by the standard electron balance equation in a "kinetics" cell, which includes many PICs, usually ~ 20. To calculate ionization process at high laser intensities, we consider both impact and optical field ionization (OFI). The OFI is included as a process of successive ionization whose probability depends on the electric field strength, E, and ionization potential of the average ion in a "kinetics" cell according to [11]. The average charge of every CP representing ions is used in the equation of motion. Because an organic hydrocarbon target is composed of two different mass components, hydrogen and carbon, we develop a two-component model to simulate distinct acceleration of hydrogen and carbon ions. In this model hydrogen is fully ionized, whereas for carbon we calculate ionization in the framework of the average ion approximation.

The 1–2/2D relativistic electromagnetic, two-component PIC code with the square current and charge weighting is used to calculate the interaction of an intense obliquely incident p-polarized pulse laser with an organic hydrocarbon solid target. Collisions are computed as an effective force after calculation of the velocity and position of CP. The calculation with movable ions is carried out for a solid with the initial density of $1\,\mathrm{g/cm^3}$. The numbers of protons and carbon ions are chosen to be equal, as in benzene. The initial charge of carbon ions $z = 1$. Simulations are performed at wavelengths of 800 nm and 400 nm for two laser intensities, $10^{17}\,\mathrm{W/cm^2}$ and $10^{18}\,\mathrm{W/cm^2}$. The laser intensity is kept constant during the pulse duration of 100 fs. The incident angle of a p-polarized pulse is 45°. The time step is set to $0.03/\omega_{\mathrm{pl}}^0$, where ω_{pl}^0 is the initial plasma frequency. The number of CPs is 5×10^4 per 1 μm of the plasma. The thickness of the thin layer is set to be 25 nm as suggested by the results of MD simulations. The spalled layer is irradiated by the femtosecond laser pulse at the time when it reaches the distance of 1 μm above the surface of the target.

2 Results and discussion

At the first stage of the present computational study we perform a series of large-scale MD simulations of laser irradiation of an organic sample. The conditions and microscopic mechanisms of laser-induced spallation and the fluence dependence of the parameters of the ejected layer are investigated.

We find that at low laser fluences the material ejection is limited to thermal desorption of individual molecules from the irradiated surface. For fluences higher than $\sim 25\,\mathrm{J/m^2}$ we start to observe generation of small voids or microcracks at a certain depth under the surface. At laser fluences below a threshold fluence of $29\,\mathrm{J/m^2}$ the initial void nucleation and growth do not lead to the material ejection and are followed by the collapse of the voids. Just below the threshold fluence we observe the formation of bigger voids that do not disappear with time leading to a permanent damage to the irradiated sample. As the laser fluence exceeds the threshold fluence, the void nucleation and growth lead to the spallation and ejection of a large and relatively intact layer of material.

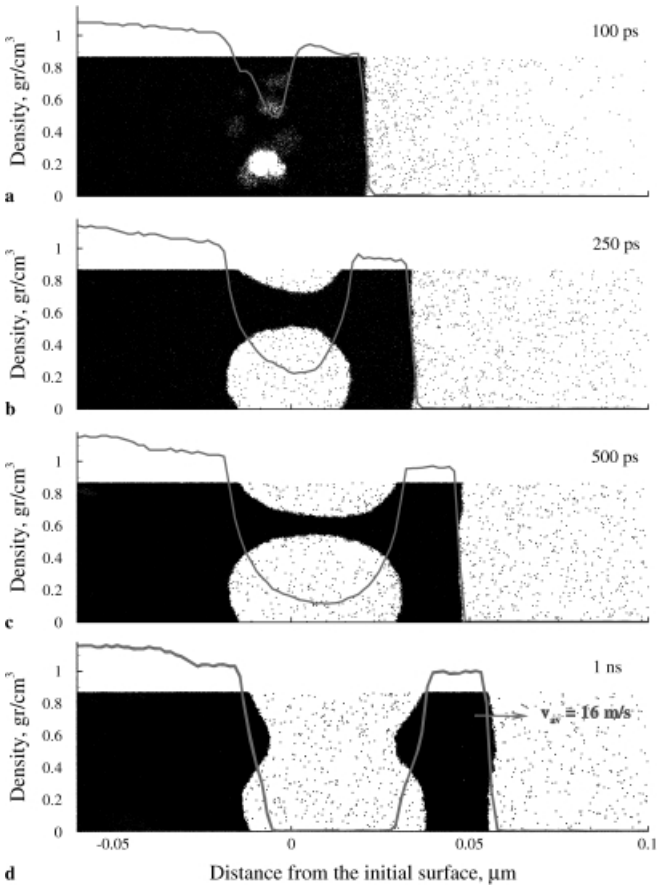

Fig. 2a–d. Density profiles near the surface of irradiated sample for simulation with 15-ps laser pulse and fluence of $31\,\mathrm{J/m^2}$. Corresponding snapshots from the simulation are shown in the background of the density plots

The dynamics of the layer spallation is illustrated by Fig. 2, where snapshots from a simulation performed at laser fluence of $31\,\mathrm{J/m^2}$ are shown. In this simulation we observe that shortly after the end of the laser pulse a few voids are nucleated at a certain depth under the irradiated surface. The snapshots taken at 100 ps, 200 ps, and 500 ps show a fast growth of one of the voids that eventually leads to the separation of a large surface layer from the bulk of the sample, as shown by the snapshot at 1000 ps. The number of molecules in the ejected layer corresponds to the 16-nm layer of the original sample. By the time of 1 ns the layer is located at 50 nm above the original surface of the target and is moving from the target with a velocity of 16 m/s. The density of the gas-phase molecules between the layer and the remaining target is $\sim 1.5 \times 10^{19}\,\mathrm{molecules/cm^3}$ which is less than the density of an ideal gas under normal conditions. The velocity of the layer, therefore, will not be affected by the expansion of the gas phase and will remain constant at later times. The average temperature of the layer is 726 K, a value below the melting temperature of the model material, 750 K. An apparent viscous, liquid-like behavior observed in Fig. 2 can be explained by the tensile stresses in the region of void formation that can locally reduce the melting temperature of the material [31].

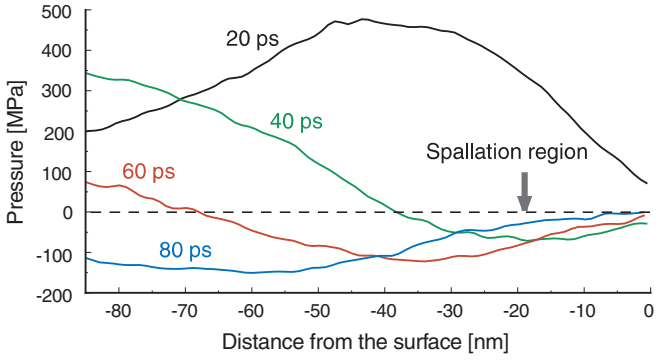

Fig. 3. The spatial distribution of pressure in the MD computational cell at different times following irradiation by 15-ps laser pulse at laser fluence of 31 J/m^2. Snapshots from the simulation are shown in Fig. 2. Non-reflecting boundary condition is applied at the depth of −90 nm as shown in Fig. 1

It is evident from the low temperature of the ejected layer and from the visual analysis of the snapshots given in Fig. 2 that the physical processes leading to the material ejection have a mechanical rather than thermal character. We find that the condition of stress confinement, realized in the present simulations, results in the buildup of a high pressure within the absorbing region during the laser pulse. The pressure buildup can be seen in Fig. 3, where the spatial distribution of the local hydrostatic pressure in the irradiated sample is shown for different times. A maximum compressive pressure as high as 470 MPa is reached in the absorption region shortly after the end of the laser pulse. Interaction of the laser-induced pressure with the free surface leads to the development of the tensile component of the pressure wave propagating from the absorption region deeper into the sample. In the case of elastic material response the tensile component would increase with depth and would reach a maximum value equal to the compressive component at approximately one penetration depth beneath the surface [24, 32]. In the simulations performed at laser fluences above the threshold fluence, however, the tensile pressure exceeds the dynamic tensile strength of the material [33] and causes mechanical fracture or spallation. The amplitude of the tensile component of the pressure wave is defined in this case by the dynamic tensile strength of the material and can be significantly lower than the one of the compressive component. In particular, for the simulation performed at laser fluence of 31 J/m^2, a maximum tensile pressure of −150 MPa has been detected, Fig. 3. The microscopic mechanism of spallation observed in the simulations and consisting of nucleation, growth and coalescence of voids is in a qualitative agreement with a recent theoretical model proposed in [33] for the spallation at high strain rates.

The depth of the void nucleation and spallation, marked in Fig. 3, is significantly closer to the surface than the depth at which the maximum tensile stresses are reached, ∼ 50 nm or approximately one penetration depth beneath the surface. This observation can be explained by the strong temperature dependence of the ability of material to support tensile stresses. The tensile strength of the material heated by laser irradiation decreases significantly as the temperature approaches the melting temperature. The depth of the photomechanical damage, marked in Fig. 3, is determined therefore by the balance between the tensile pressure that is increasing with depth and reaches −90 MPa in the spallation region and the decreasing thermal softening due to the laser heating. Although a significantly higher tensile pressure, up to −150 MPa, is reached deeper in the sample, Fig. 3, it does not cause mechanical fracture of the colder and stronger material.

In simulations performed with higher laser fluences the void nucleation is observed not only at the depth defined by the balance between the increasing tensile stresses and the thermal softening, but over a larger volume in the surface region. This can be illustrated by snapshots from the simulation at laser fluence of 34 J/m^2 shown in Fig. 4. In this simulation short pulse laser irradiation leads to the void nucleation within a wide surface region, Fig. 4a. At later times the deeper voids continue to grow, coalesce, and, at 700 ps, a large surface layer is separated from the sample, Fig. 4d. The number of molecules in the ejected layer corresponds to the 23-nm layer of the original sample, the average velocity of the layer is 71 m/s, the density of the gas phase molecules between the layer and the remaining target is $\sim 2 \times 10^{19}$ molecules/cm^3, and the average temperature of the layer is 757 K, close to the melting temperature of the model material. Note that the mechanical stability of the surface region subjected to the void nucleation is strongly affected by the laser heating and the analytical prediction on the formation of multiple spallation planes [32] in the absorption region cannot be directly applied for the quantitative description of the simulation results.

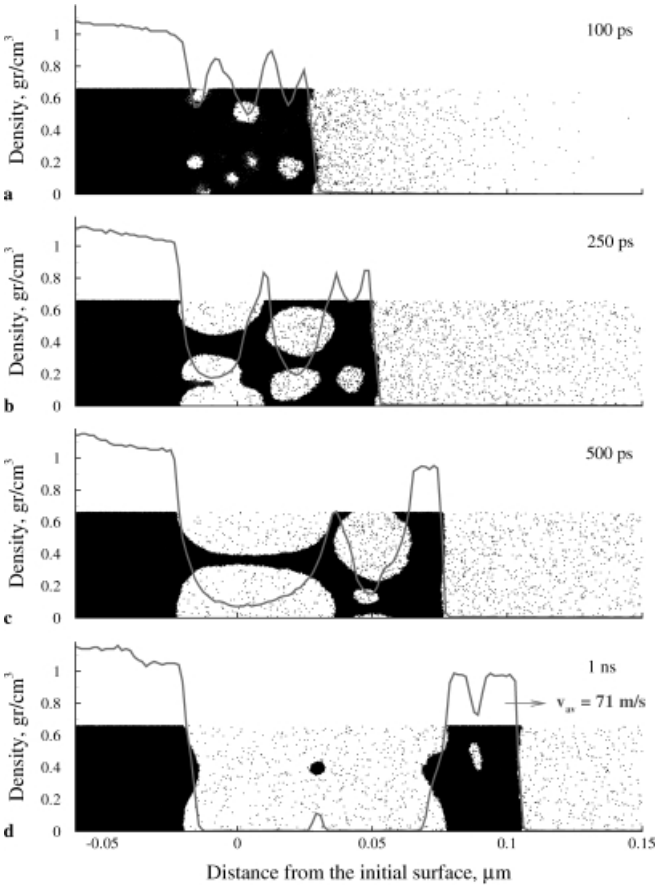

Fig. 4a–d. Density profiles near the surface of irradiated sample for simulation with 15-ps laser pulse and fluence of 34 J/m^2. Corresponding snapshots from the simulation are shown in the background of the density plots

For simulations performed in the stress-confinement irradiation regime the spallation of a surface layer of the sample is found to be the dominant process of laser ablation in a relatively wide range of fluences, from $\sim 29\,\mathrm{J/m^2}$ up to $\sim 35\,\mathrm{J/m^2}$. At higher laser fluences the ejected material decomposes into liquid droplets and individual molecules with the fraction and the average size of the droplets decreasing with fluence [21, 23]. In the simulations performed with longer times, 150 ps, when the stress confinement condition is not satisfied, the photomechanical effects do not play any significant role in the material ejection and no layer spallation is observed at any fluence [20].

The MD simulations described above and illustrated by Figs. 2 and 4 have been performed for 1 ns starting from the beginning of the laser pulses. By the end time of the simulations the ejected layers are moving with constant velocities and their relatively low temperatures suggest that the layers will maintain their integrity and temperature at least on the timescale of tens of ns. This makes it straightforward to extrapolate the density plots shown in Figs. 2 and 4 to the times when the layers reach the position of 1 μm above the remaining target. The extrapolation gives the times of 62 ns and 13 ns for the simulations shown in Figs. 2 and 3, respectively. By that time we can estimate the temperature of the surface of the remaining target to be 550 K and 580 K, the thickness of the layers to be 20.5 nm and 27.7 nm, and the density of both layers to be $1\,\mathrm{g/cm^2}$. The extrapolated density profiles and the parameters of the layers are used as input data for the PIC simulations of further interaction with an intense femtosecond laser pulse.

In the second part of the present computational study we simulate interaction of a short second-harmonic laser pulse with the thin spalled layer. We choose the second-harmonic light to avoid the effect of the amplified spontaneous emission (prepulse), the duration of which can exceed 1–2 ns [34]. Though having a low contrast ratio $1 : 10^{6-7}$, such a prepulse might destroy the layer before the main short laser pulse comes. In the case of the second harmonics, the contrast ratio can be reduced to $1 : 10^{9-12}$ with a negligible effect on the layer dynamics.

The temporal evolution of the absorption rate of a laser pulse at $\lambda = 400\,\mathrm{nm}$ is shown in Fig. 5. The rate is considerably high, about 30% for both laser intensities. Because the layer thickness is initially comparable to the skin depth, the transmittance of the layer is high, as seen in Fig. 6. A large amount, about 10%, of the laser energy passes through the layer. The transmitted light is absorbed at the surface of the target and at the rear side of the layer. As the layer of material getting fully ionized, the density of the plasma increases by a factor of three and the skin depth, $d \sim \pi/\omega_{\mathrm{pl}}$, decreases. This leads to a higher absorption rate and a weaker plasma transmittance. At lower laser intensity, the absorption process

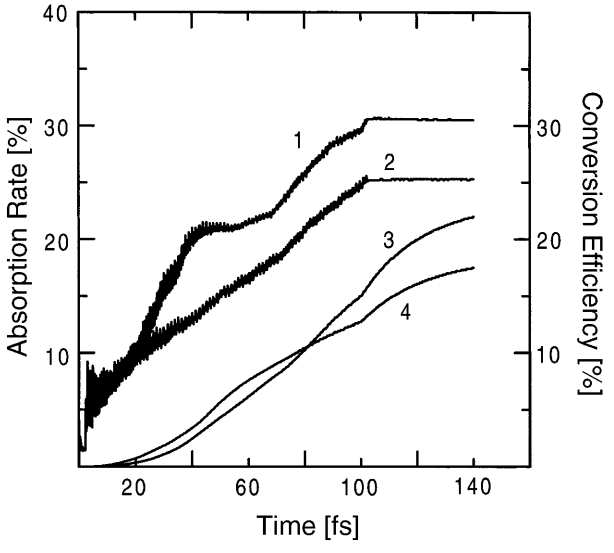

Fig. 5. Temporal evolution of the absorption rate, (1) and (2), and the conversion efficiency of the energy of the laser pulse to the energy of ions, (3) and (4), for a 25-nm spalled layer, separated by 1 μm from the target and irradiated with 100-fs laser pulse at wavelength of 400 nm and intensity of $10^{17}\,\mathrm{W/cm^2}$, (1) and (3) and $10^{18}\,\mathrm{W/cm^2}$, (2) and (4)

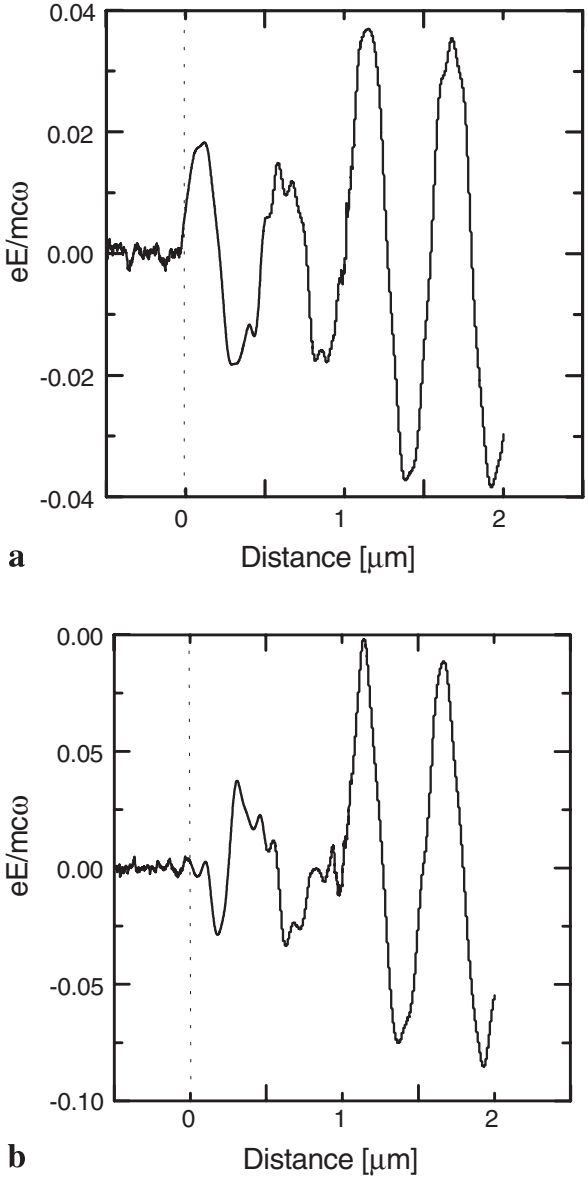

Fig. 6a,b. Spatial distribution of the laser field in the layer–solid system after 20 fs, **a** $I = 10^{17}\,\mathrm{W/cm^2}$ and **b** $I = 10^{18}\,\mathrm{W/cm^2}$. Here, and in the following figures, the surface of the solid is marked by the *dashed line*, the spalled layer is originally located at 1 μm above the surface

could be attributed to the resonance absorption [35], whereas at the laser intensity of 10^{18} W/cm^2, the resonance absorption hardly occurs. We believe that the high absorption rate is sustained by the ion acceleration. An electrostatic field at three cliff boundaries in this system dominates the conversion efficiency to ions. Hot electrons produced by the laser pulse create strong electrostatic field at the plasma boundaries. This field is dominant in the ion acceleration. In the absence of the spalled layer, the absorption rate for a bulk target irradiated by a 100-fs laser pulse with the intensity of 10^{18} W/cm^2 would be about 2%–6% [36]. With the layer, the conversion efficiency – the ratio of the ion energy to the laser energy – weakly depends on the laser intensity and exceeds 20% shortly after the end of the laser pulse, Fig. 5.

The plasma electrostatic field averaged over the pulse duration is shown in Fig. 7. The maximum strength of the field is reached at the layer boundaries. Because the layer thickness is much smaller than the hot electron excursion length, the electric field is high at the front surface of the layer and at the rear surface. The electric field can exceed 10 GV/cm, which leads to the appearance of energetic ions.

The spatial distribution of ion velocities is shown in Fig. 8 for carbon ions and protons for different laser intensities. The maximum energy of forwardly accelerated carbon ions reaches 5 MeV at laser intensity of 10^{18} W/cm^2, whereas the maximum proton energy is only 0.8 MeV. The maximum ion energy is determined by the potential difference, $\Delta\Phi$, which is restrained by the gap between the layer and the surface of the solid, as the electrostatic field inside the solid is zero. Because of rapid ionization, the carbon ions are nearly fully ionized with charges $z \sim 5$–6 during the first 30 fs of the laser pulse. Carbon ions acquire higher energy, $ez\Delta\Phi$, for two reasons: first, they have higher charges, and second, having lower velocities than protons, they experience higher potential difference created by the end of the pulse, when light protons are already gone. The spatial velocity distribution is symmetric in contrast to results

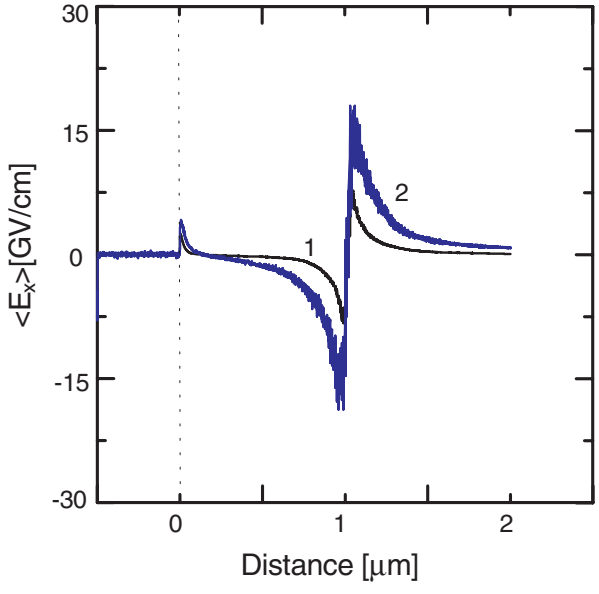

Fig. 7. Spatial distribution of the temporary averaged electric field, (1) $I = 10^{17}$ W/cm^2 and (2) $I = 10^{18}$ W/cm^2

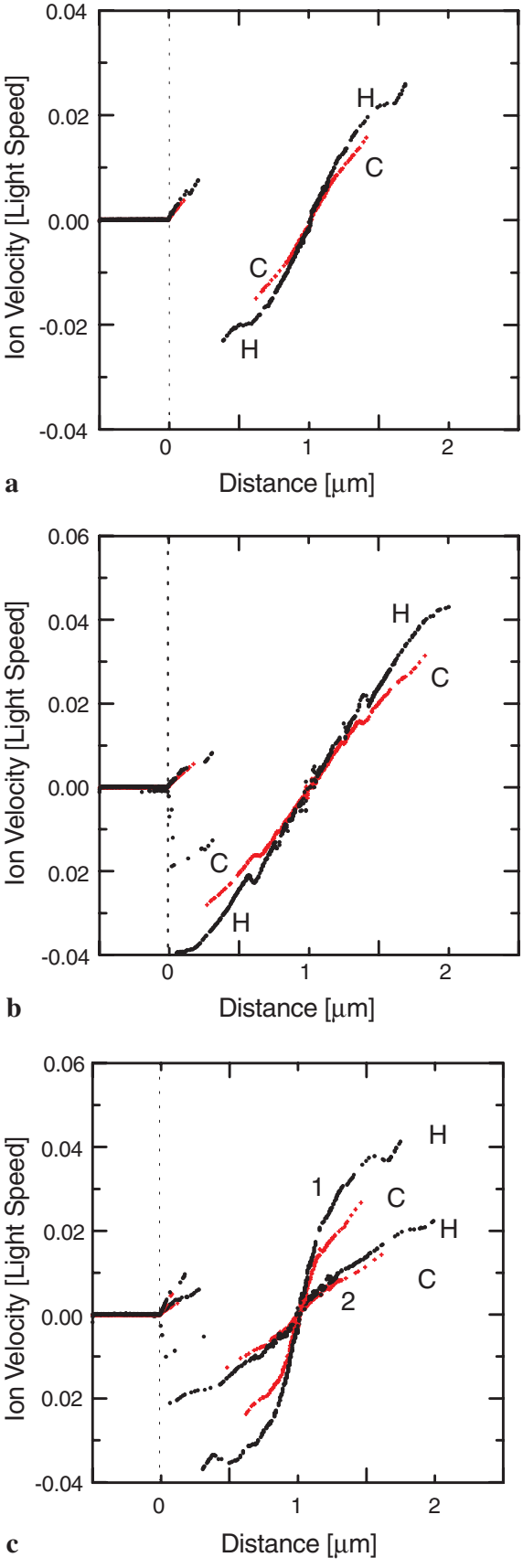

Fig. 8a–c. Spatial distribution of the velocities of carbon ions (*grey crosses*) and protons (*black points*) just after the end of the laser pulse. Data is given for **a** $\lambda = 400$ nm, $I = 10^{17}$ W/cm^2, **b** $\lambda = 400$ nm, $I = 10^{18}$ W/cm^2, and **c** $\lambda = 800$ nm and intensities (1) $I = 10^{18}$ W/cm^2 and (2) $I = 10^{17}$ W/cm^2

of [1, 2, 9], and maximum energies of backwardly accelerated ions are close to those of forwardly accelerated ones. This is also the effect of restriction of the potential difference by the finite gap. The maximum energy of hot electrons producing the potential difference is limited by the gap. Energetic electrons penetrate into the solid so that there are no hot electrons with energy $\varepsilon > \Delta\Phi$. The transmitted portion of the laser light creates plasma on the surface of the target. As a result, a certain number of ions are accelerated backward, as seen in Fig. 8 at distances close to the surface. In spite of the higher effective strength of the laser field, $E = eE/m\omega c$, the velocity distributions obtained for a laser pulse with wavelength $\lambda = 800\,\mathrm{nm}$ are similar to the ones observed in simulations with the second harmonics due to the finite potential difference at the gap. This means that the energy loss due to the use of the second harmonics is determined by the conversion efficiency from ω to 2ω only.

3 Conclusion

The results of the present computational study demonstrate the feasibility of the proposed method for an efficient generation of energetic ions near a target sample. We show that a direct irradiation of a bulk organic sample by a laser prepulse performed in the regime of stress confinement can lead to the ejection of a layer of relatively intact material with thickness determined by the laser penetration depth and fluence. The further irradiation of the spalled layer by an obliquely incident p-polarized, second-harmonic laser pulse leads to an efficient emission of carbon ions with energies over 1 MeV and protons with energy up to 1 MeV even at a modest intensity of $10^{17}\,\mathrm{W/cm^2}$. The distance between the spalled layer and the target is controlled by the delay between the first and the second pulses and can be optimized for the maximum intensity of the ion beam. A transient electrostatic field generated between the layer and the surface of the target can be up to $10\,\mathrm{GV/cm}$ and the efficiency of the conversion of the laser energy to the energy of the ions can be as high as 20% for all ions and 10% for ions with energy above 1 MeV.

Acknowledgements. L.V.Z. would like to thank the Foreign Researcher Inviting Program of the Japan Atomic Energy Research Institute and Hiroshi Fukumura for their hospitality. Partial support of this work was provided by the US Office of Naval Research through the Medical Free Electron Laser Program. Partial computational support was provided by IBM-SUR Program, the NSF-MRI Program. T.T. is supported by USDoE contract W-7405-Eng.-4P. We would like to thank Barbara Garrison for insightful and stimulating discussions.

References

1. A.G. Zhidkov, A. Sasaki, T. Tajima: Rev. Sci. Instrum. **71**, 931 (2000)
2. A.G. Zhidkov, A. Sasaki, T. Tajima: Phys. Rev. E **61**, R2224 (2000)
3. V.S. Letokhov, E.A. Yukov: Laser Phys. **4**, 382 (1994)
4. A.V. Andreev, R.V. Volkov, V.M. Gordienko: JETP Lett. **69**, 371 (1999)
5. B. Harss et al.: Phys. Rev. Lett. **82**, 3964 (1999)
6. J. Denavit: Phys. Rev. Lett. **69**, 3052 (1992)
7. S.J. Gitomer, R.D. Jones, F. Begay, A.W. Ehler, J.F. Kephart, R. Kristal: Phys. Fluids **29**, 2679 (1986)
8. A.P. Fews, P.A. Norreys, F.N. Beg, A.R. Bell, A.E. Dangor, C.N. Danson, P. Lee, S.J. Rose: Phys. Rev. Lett. **73**, 1801 (1994)
9. F.N. Beg, A.R. Bell, A.E. Dangor, C.N. Danson, A.P. Fews, M.E. Glinsky, B.A. Hammel, P. Lee, , P.A. Norreys, M. Tatarakis: Phys. Plasmas **4**, 447 (1997)
10. A.G. Zhidkov, A. Sasaki, T. Tajima, T. Auguste, P. D'Olivera, S. Hulin, P. Monot, A.Ya. Faenov, T.A. Pikuz, I.Yu. Skobelev : Phys. Rev. E **60**, 3273 (1999)
11. A. Zhidkov, A. Sasaki: Phys. Plasmas **7**, 1341 (2000)
12. S.P. Hatchett et al.: Phys. Plasmas **7**, 2076 (2000)
13. A. Maksimchuk, S. Gu, K. Flippo, D. Umstadter, V.Yu. Bychenkow: Phys. Rev. Lett. **84**, 4108 (2000)
14. E.L. Clark, K. Krushelnick, M. Zepf, F.N. Beg, M. Tatarakis, A. Machacek, M.I.K. Santala, I. Watts, P.A. Norreys, A.E. Dangor: Phys. Rev. Lett. **85**, 1654 (2000)
15. R.L. Webb, J.T. Dickinson, G.J. Exarhos: Appl. Spectrosc. **51**, 707 (1997)
16. B.N. Kozlov, B.A. Mamyrin: Tech. Phys. **44**, 1073 (1999)
17. J. Heitz, J.T. Dickinson: Appl. Phys. A **68**, 515 (1999)
18. M. Handschuh, S. Nettesheim, R. Zenobi: Appl. Surf. Sci. **137**, 125 (1999)
19. K.H. Song, X. Xu: Appl. Surf. Sci. **127-129**, 111 (1998)
20. L.V. Zhigilei, B.J. Garrison: Appl. Phys. Lett. **74**, 1341 (1999)
21. L.V. Zhigilei, B.J. Garrison: Appl. Phys. A **69**, 75 (1999)
22. E. Hare, J. Franken, D.D. Dlott: J. Appl. Phys. **77**, 5950 (1995)
23. L.V. Zhigilei, B.J. Garrison: J. Appl. Phys. **88**, 1281 (2000)
24. I. Itzkan, D. Albagli, M.L. Dark, L.T. Perelman, C. von Rosenberg, M.S. Feld: Proc. Natl. Acad. Sci. USA **92**, 1960 (1995)
25. R.E. Johnson: In *Large Ions: Their Vaporization, Detection and Structural Analysis*, ed. by T. Baer, C.Y. Ng, I. Powis (Wiley, New York, 1996) p. 49
26. J.R. Brock, M.F. Becker, J.W. Keto: US Patent #5,585,020 (Dec. 17, 1996)
27. L.V. Zhigilei, P.B.S. Kodali, B.J. Garrison: J. Phys. Chem. B **101**, 2028 (1997); ibid. **102**, 2845 (1998)
28. L.V. Zhigilei, B.J. Garrison: Mater. Res. Soc. Proc. **538**, 491 (1999)
29. A.G. Zhidkov: Phys. Plasmas **5**, 385 (1998)
30. A. Zhidkov, A. Sasaki: Phys. Rev. E **59**, 7085 (1999)
31. J. Wang, J. Li, S. Yip, D. Wolf, S. Phillpot: Physica A **240**, 396 (1997)
32. R.S. Dingus, R.J. Scammon: SPIE Proc. Series **1427**, 45 (1991)
33. E. Dekel, S. Eliezer, Z. Henis, E. Moshe, A. Ludmirsky, I.B. Goldberg: J. Appl. Phys. **84**, 4851 (1998)
34. J.D. Kmetec, C.L. Gordon, III, J.J. Macklin, B.E. Lemoff, G.S. Brown, S.E. Harris: Phys. Rev. Lett. **68**, 1527 (1992)
35. S. Bastiani, A. Rousse, J.P. Geindre, P. Audebert, C. Quoix, G. Hamoniaux, A. Antonetti, J.-C. Gauthier: Phys. Rev. E **56**, 7179 (1997)
36. W.S. Lawson, P.W. Rambo, D.J. Larson: Phys. Plasmas **4**, 788 (1997)